



Enhanced joint remote state preparation under correlated amplitude damping decoherence by weak measurement and quantum measurement reversal

Jia-yin Peng^{1,2,3,4}, Zhen Yang^{2,3}, Liang Tang^{5,a}

¹ School of Mathematics and Statistics, Yili Normal University, Yili 835000, China

² Institute of Intelligent Information and Quantum Information, Sichuan Normal University, Chengdu 610066, China

³ School of Mathematical Sciences, Sichuan Normal University, Chengdu 610066, China

⁴ School of Mathematics and Information Science, Neijiang Normal University, Neijiang 641100, Sichuan, China

⁵ School of Science, Xihua University, Chengdu 610039, China

Received: 28 December 2022 / Accepted: 17 April 2023

© The Author(s), under exclusive licence to Società Italiana di Fisica and Springer-Verlag GmbH Germany, part of Springer Nature 2023

Abstract A joint remote state preparation (JRSP) scheme is put forward to prepare an arbitrary single-qubit state. Specifically, the GHZ-state of three qubits as a resource successively passes through the correlated amplitude damping (CAD) noisy channel. Then, an analytical expressions quantifying the average fidelity of JRSP is obtained under the CAD noisy channel. Comparing with the results of uncorrelated amplitude damping (AD) noise, we find that the correlated effects enable to improve the average fidelity of JRSP in the CAD noisy channel. Furthermore, by introducing the weak measurement (WM) and quantum measurement reversal (QMR), and we calculate the average fidelity as a function of the decoherence strength, memory parameter, measurement strength of WM and measurement strength of QMR for an arbitrary quantum state to be prepared. These results demonstrate that the combination of WM and QMR can significantly improve the average fidelity in both uncorrelated and correlated AD noise. Our results may extend the capabilities of WM as a technique in various quantum information processing which are affected by correlated noise.

1 Introduction

One of the key tasks of quantum information [1–4] is the use of entangled states to transmit information in quantum systems. The striking characteristic of entanglement [5–7] enables communication methods completely different from classical ones. As the most well-known example of quantum communication, quantum teleportation (QT) was first proposed by Bennet et al. [8], which allows one to convey an arbitrary single quantum state from the sender to a distant receiver via consuming one ebit and two cbits. In order to reduce the classical resources required in QT, the first remote state preparation (RSP) scheme was first put forward by Pati [9] in 2000, where the sender and the receiver share one ebit of entanglement in advance, and the sender holds all the classical information of the target state. This RSP is completed probabilistically after the sender's single-qubit von Neumann measurement and the receiver's recovery operation. After Pati's pioneering work, much attention is focused on RSP in both theoretical [10–15] and experimental [16–18] aspects. In the RSP scheme, the information transmitted remotely is assigned to only one sender, which may lead to information disclosure when the sender is dishonest.

In order to address this deficiency, JRSP was proposed by increasing the number of senders [19, 20]. In the process of JRSP, the teleported information is broken up into several parts, all of the senders must cooperate to aid the receiver to restore the target state. It means that neither a single sender nor part of the senders can help the receiver to reconstruct the target state, thus the JRSP can improve the communication security. Due to the remarkable advantage, JRSP has attracted great interest since its first appearance, and different entangled states, like Bell, GHZ, W, cluster and Brown states, are used as shared resource in JRSP [21–28]. The JRSP containing some special quantum states, such as four-dimensional GHZ-type state [29], cluster-type [30, 31], W-type [32], equatorial two-qudit state [33, 34] and more, are investigated. In 2012, Luo et al. [18] proposed the experimental architecture of JRSP using GHZ state. Nguyen et al. [35] presented the quantum circuit of JRSP by using POVM measurement. Yu et al. [36] designed the schemes for JRSP of arbitrary two- and three-photon states with linear-optical elements. It is easy to find that all of the JRSP schemes above are considered in an ideal environment. However, quantum noise is an unavoidable phenomenon in realistic environment. Noise can decohere a quantum entangled state, in which case the output state received is inconsistent with the prepared state. In other words, the entanglement is fragile and easily broken via environmental noise. Therefore, it is meaningful to study the influence of noise on JRSP.

^a e-mail: tangliang233@126.com (corresponding author)

Each physical process, as we all know, can be viewed as a quantum channel, which maps the initial state of the system to the final state [8, 37]. For multipartite quantum systems or consecutive uses of the same channel, these channels can be divided into correlated or uncorrelated channel. The effect of the uncorrelated noise on JRSP has been widely studied by a number of researchers [38–46]. Nevertheless, the correlated channel is more practical in physical process, especially, in the case of high transmission rate [47–49]. Unlike the uncorrelated AD channel in which each qubit independently experiences the noise, the qubits may suffer relaxation simultaneously in the CAD channel [50]. As shown in Ref. [51], the correlation effects help to avoid entanglement sudden death. However, to the best of our knowledge, few detailed investigations involving the influence of CAD on JRSP are available at the present. On the other hand, to overcome the impact of decoherence on quantum entanglement, several types of decoherence suppression methods have been proposed, including dynamical decoupling [52], quantum entanglement purification [53], quantum error coding [54], and decoherence-free subspace [55].

As an important quantum technology, weak measurement (WM) has attracted extensive attention in the past few years [51, 56–60]. Different from the traditional von Neumann orthogonal projection measurement, WM can not completely collapse the measured quantum system, and it is more gentle in extracting information from the system. Thus, we can use quantum measurement reversal (QMR) to restore the initial state with a certain probability. Recently, some researchers have found the ability of WM and QMR to protect entanglement from AD noise [57, 59, 61–69]. To be specific, it needs repeatedly measurement to gain an unknown state information with a finite probability. The probability of success decreases with increasing strength of the measurement. Meanwhile, the action that accompanies the weak measurement is the quantum measurement reversal (QMR), which utilized to erase the influence of the first measurement [65]. In 2008, Katz et al. [66] discussed the relationship between the fidelity and the strength of the measurement in the system of superconducting qubit. Then, Kim et al. [67] utilized the form of operator to describe the process of weak measurement and recover measurement in 2009. They also researched the feasibility of utilizing weak measurement method in the system of photonic qubit. Whereafter, in 2011, Kim et al. [68] proposed the weak measurement method can resist the decoherence phenomenon of single (two)-qubit entangled state in AD channel, and Lee et al. [69] demonstrated it in experimental. However, no systematic study devoted to the application of WM and QMR with CAD noise on JRSP protocol has been reported yet. This motivates us to utilize WM and QMR to study the JRSP under CAD noise. More importantly, we also need to know whether WM and QMR can suppress the influence of CAD noise on JSRP protocol.

In this paper, we firstly consider the influence of CAD noise on JRSP, and then propose a scheme to improve the average fidelity with the help of WM and QMR. We find that the average fidelity of JRSP under CAD noise is better than that under AD noise. In addition, we also show that the combined WM and QMR can greatly improve the average fidelity in both AD and CAD noise. In particular, for the completely uncorrelated AD and fully correlated amplitude damping (FCAD), the average fidelity may be close to 1.

The rest of this paper is organized as follows. In Sect. 2, the JRSP via three-qubit entangled GHZ-state as quantum channel under CAD noise is investigated in detail. Then in Sect. 3, we show that how to use WM and QMR to improve average fidelity of JRSP. Finally, some conclusions are drawn in Sect. 4.

2 JRSP under CAD

In this section, we investigate JRSP under CAD for an unknown single-qubit state. The scheme involves totally three parties located in different places: two observers Alice and Bob, and a receiver Charlie. Suppose that two senders Alice and Bob would like to help the receiver Charlie prepare an arbitrary unknown single-qubit state $|\xi\rangle$, which can be given by

$$|\xi\rangle = \cos \frac{\theta}{2} |0\rangle + \sin \frac{\theta}{2} e^{i\phi} |1\rangle, \quad (1)$$

where θ and ϕ are the polar and the phase parameters, respectively, and satisfy $\theta \in [0, \pi]$ and $\phi \in [0, 2\pi]$. Alice and Bob own the information of amplitude and phase factor, respectively. Assumed that Alice holds a quantum resource generator in her laboratory and she generates the three-qubit entangled GHZ-state, such that

$$|\mathcal{G}\rangle_{ABC} = \frac{1}{\sqrt{2}}(|000\rangle + |111\rangle)_{ABC}, \quad (2)$$

and sends qubit B and C to Bob and Charlie through channel with CAD noise successively, respectively. Due to the consecutive uses of the noisy channel, the correlated effect should be considered. Therefore, the entangled state $|\mathcal{G}\rangle_{ABC}$ has suffered CAD noise during the distribution. The dynamics of an entangled state subject to CAD noise is described by the quantum super-operation ε acting on the initial state [60].

$$\varepsilon_{CAD}(\rho) = (1 - \mu) \sum_{i,j=0}^1 (I \otimes E_{ij}) \rho (I \otimes E_{ij})^\dagger + \mu \sum_{k=0}^1 (I \otimes A_k) \rho (I \otimes A_k)^\dagger, \quad (3)$$

where I is a second-order identity matrix, μ is the correlated parameter (memory parameter) with $0 \leq \mu \leq 1$, and

$$\rho = |\mathcal{G}\rangle_{ABC} \langle \mathcal{G}| = \frac{1}{2}(|000\rangle + |111\rangle)_{ABC} (\langle 000| + \langle 111|). \tag{4}$$

Obviously, we can obtain the uncorrelated AD channel by $\mu = 0$ and get the FCAD channel when $\mu = 1$. $E_{ij} = E_i \otimes E_j$ is the tensor product for Kraus operators of AD noise. The corresponding Kraus operators are

$$E_0 = \begin{pmatrix} 1 & 0 \\ 0 & \sqrt{1-\gamma} \end{pmatrix}, \quad E_1 = \begin{pmatrix} 0 & \sqrt{\gamma} \\ 0 & 0 \end{pmatrix}, \tag{5}$$

the parameter γ is the decoherence strength of the AD channel and $0 \leq \gamma \leq 1$. A_k has been solved by studying the correlated Lindblad equation [61], which gives the following formalism

$$A_0 = \begin{pmatrix} 1 & 0 & 0 & 0 \\ 0 & 1 & 0 & 0 \\ 0 & 0 & 1 & 0 \\ 0 & 0 & 0 & \sqrt{1-\gamma} \end{pmatrix}, \quad A_1 = \begin{pmatrix} 0 & 0 & 0 & \sqrt{\gamma} \\ 0 & 0 & 0 & 0 \\ 0 & 0 & 0 & 0 \\ 0 & 0 & 0 & 0 \end{pmatrix}. \tag{6}$$

The evolution of the initially shared state in Eq. (2) under the CAD noise can be obtained from Eqs. (3–5), which is expressed as

$$\begin{aligned} \varepsilon_{CAD}(\rho) = & \frac{1}{2} [|000\rangle\langle 000| + (\bar{\mu}\bar{\gamma} + \mu\sqrt{\bar{\gamma}})(|000\rangle\langle 111| + |111\rangle\langle 000|) \\ & + (\bar{\mu}\bar{\gamma}^2 + \mu\bar{\gamma})|111\rangle\langle 111| + \bar{\mu}\bar{\gamma}\gamma(|110\rangle\langle 110| + |101\rangle\langle 101|) \\ & + (\bar{\mu}\bar{\gamma}^2 + \mu\gamma)|100\rangle\langle 100|]_{ABC}, \end{aligned} \tag{7}$$

where $\bar{\mu} = 1 - \mu$ and $\bar{\gamma} = 1 - \gamma$. Our scheme includes the following three steps:

Step 1. Alice implements a single qubit von Neumann measurement with the basis $\mathcal{M}\mathcal{A} = \{\mathcal{M}\mathcal{A}_0, \mathcal{M}\mathcal{A}_1\}$ on qubit A , where

$$\mathcal{M}\mathcal{A}_0 = \left(\cos \frac{\theta}{2} |0\rangle + \sin \frac{\theta}{2} |1\rangle \right) \left(\cos \frac{\theta}{2} \langle 0| + \sin \frac{\theta}{2} \langle 1| \right) \tag{8}$$

and

$$\mathcal{M}\mathcal{A}_1 = \left(\sin \frac{\theta}{2} |0\rangle - \cos \frac{\theta}{2} |1\rangle \right) \left(\sin \frac{\theta}{2} \langle 0| - \cos \frac{\theta}{2} \langle 1| \right). \tag{9}$$

After the measurement, Alice encodes the result in classical bit m and sends it to Bob and Charlie via the classical channel. The system state after Alice’s measurement is

$$\rho_m = \text{tr}_A \left[\frac{\mathcal{M}\mathcal{A}_m \varepsilon_{CAD}(\rho) (\mathcal{M}\mathcal{A}_m)^\dagger}{\text{tr}(\mathcal{M}\mathcal{A}_m \varepsilon(\rho) (\mathcal{M}\mathcal{A}_m)^\dagger)} \right], \quad \text{with } m \in \{0, 1\}. \tag{10}$$

Step 2. Bob performs a single qubit von Neumann measurement with the basis $\mathcal{M}\mathcal{B}_m = \{\mathcal{M}\mathcal{B}_m^0, \mathcal{M}\mathcal{B}_m^1\}$ on qubit B according to Alice’s result m , where $\mathcal{M}\mathcal{B}_m^0 = |O_m^0\rangle\langle O_m^0|$ and $\mathcal{M}\mathcal{B}_m^1 = |O_m^1\rangle\langle O_m^1|$, and $\{|O_m^n\rangle : n \in \{0, 1\}\}$ are in the form

$$\begin{pmatrix} |O_m^0\rangle \\ |O_m^1\rangle \end{pmatrix} = V_m \begin{pmatrix} |0\rangle \\ |1\rangle \end{pmatrix} \tag{11}$$

with

$$V_0 = \frac{1}{\sqrt{2}} \begin{pmatrix} 1 & e^{-i\phi} \\ 1 & -e^{-i\phi} \end{pmatrix} \quad \text{and} \quad V_1 = \frac{1}{\sqrt{2}} \begin{pmatrix} e^{-i\phi} & 1 \\ -e^{-i\phi} & 1 \end{pmatrix}. \tag{12}$$

Then, he informs Charlie his measurement result n . The system state after Bob’s measurement result is

$$\rho_m^n = \text{tr}_B \left[\frac{\mathcal{M}\mathcal{B}_m^n \rho_m (\mathcal{M}\mathcal{B}_m^n)^\dagger}{\text{tr}(\mathcal{M}\mathcal{B}_m^n \rho_m (\mathcal{M}\mathcal{B}_m^n)^\dagger)} \right], \quad \text{with } m, n \in \{0, 1\}. \tag{13}$$

Step 3. According to Alice’s and Bob’s measurement results, Charlie can construct the state $|\xi\rangle$ by performing the recovery operator R_m^n , where $R_0^0 = |0\rangle\langle 0| + |1\rangle\langle 1|$, $R_0^1 = |0\rangle\langle 0| - |1\rangle\langle 1|$, $R_1^0 = |0\rangle\langle 1| - |1\rangle\langle 0|$ and $R_1^1 = |0\rangle\langle 1| + |1\rangle\langle 0|$.

After the above three steps, Charlie finally obtains the output state $\rho_m^n(out) = R_m^n \rho_m^n (R_m^n)^\dagger$, which can be given by

$$\begin{aligned} \rho_0^0(out) = \rho_0^1(out) &= \left(\cos^2 \frac{\theta}{2} + \gamma \sin^2 \frac{\theta}{2} \right) |0\rangle\langle 0| + \bar{\gamma} \sin^2 \frac{\theta}{2} |1\rangle\langle 1| \\ &+ (\overline{\mu\gamma} + \mu\sqrt{\bar{\gamma}}) \sin \frac{\theta}{2} \cos \frac{\theta}{2} (e^{-i\phi} |0\rangle\langle 1| + e^{i\phi} |1\rangle\langle 0|), \\ \rho_1^0(out) = \rho_2^1(out) &= \left(\sin^2 \frac{\theta}{2} + \gamma \cos^2 \frac{\theta}{2} \right) |1\rangle\langle 1| + \bar{\gamma} \cos^2 \frac{\theta}{2} |0\rangle\langle 0| \\ &+ (\overline{\mu\gamma} + \mu\sqrt{\bar{\gamma}}) \sin \frac{\theta}{2} \cos \frac{\theta}{2} (e^{-i\phi} |0\rangle\langle 1| + e^{i\phi} |1\rangle\langle 0|). \end{aligned} \tag{14}$$

In the JRSP scheme, the credibility of quantum teleportation through CAD noise is usually quantified by the fidelity which measures the overlap between the initial $|\xi\rangle$ and the finally teleported state $\rho_m^n(out)$,

$$F_m^n = \langle \xi | \rho_m^n(out) | \xi \rangle, \quad \text{with } m, n \in \{0, 1\}. \tag{15}$$

Considering the fact that the output state may come up with certain probability, we invoke the average fidelity

$$F_{av} = \sum_{m,n=0}^1 q_{mn} F_m^n, \tag{16}$$

where $\{q_{mn}\}$ is the probability that the state ρ_m^n occurs. Through calculation, q_{mn} equals to $\frac{1}{4}$ for any $m, n \in \{0, 1\}$ in this section. Note that this average fidelity depends on the target state, so we call it the state dependent average fidelity.

From Eqs. (1), (14), (15) and (16), it follows that the fidelity is explicitly expressed

$$F_{av} = \frac{1}{2} \left[1 + \overline{\mu\gamma} + \mu\sqrt{\bar{\gamma}}(\sqrt{\bar{\gamma}}\cos^2\theta + \sin^2\theta) \right]. \tag{17}$$

In general, the average fidelity is determined by the target state $|\xi\rangle$ and the corresponding noise channel. Therefore, it is natural to average over all of the target state to obtain a state independent effect of the corresponding noise channel, the formula of the average fidelity is as following

$$\langle \bar{F} \rangle = \frac{1}{4\pi} \int_0^\pi \sin \theta d\theta \int_0^{2\pi} d\phi \cdot F_{av}, \tag{18}$$

this average fidelity is over all of the qubit states, thus we call it the state independent average fidelity.

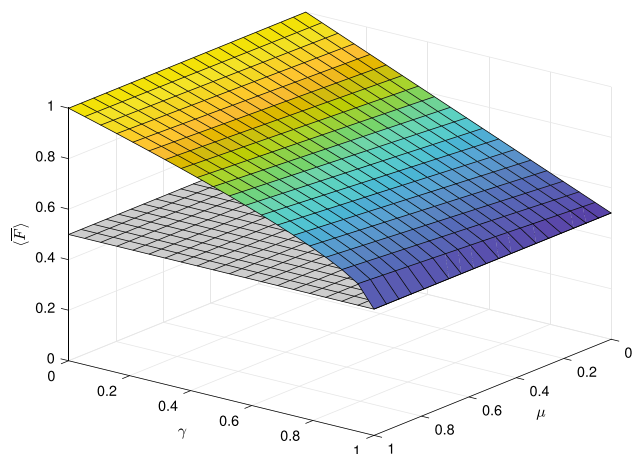
By substituting Eqs. (17) and (18), we can obtain the formula of the average fidelity

$$\langle \bar{F} \rangle = 1 + \frac{\mu}{3} (\sqrt{\bar{\gamma}} - \bar{\gamma}) - \frac{1}{2} \gamma. \tag{19}$$

The behaviors of average fidelity as a function of the parameter γ and μ are shown in Fig. 1.

As one might expect, in the uncorrelated circumstance (i.e., $\mu = 0$), the average fidelity ranges from 1 to 1/2 when the decoherence strength γ increases from 0 to 1. Specifically, in the case of $\mu = 1$, the second use has full correlation of the first use, the average

Fig. 1 The relationship among the average fidelity, the parameters γ and μ



fidelity $\langle \bar{F} \rangle$ is $(3 + \bar{\gamma} + 2\sqrt{\bar{\gamma}})/6$, which attains its maximum 1 at $\gamma = 0$ and minimum 1/2 at $\gamma = 1$. The partial derivative of $\langle \bar{F} \rangle$ with respect to the correlated parameter μ is

$$\frac{\partial \langle \bar{F} \rangle}{\partial \mu} = \frac{1}{3} \sqrt{\bar{\gamma}} (1 - \sqrt{\bar{\gamma}}) \geq 0. \tag{20}$$

That is to say that the average fidelity $\langle \bar{F} \rangle$ is increasing with the correlated parameter μ regardless of the noise parameter γ . The average fidelity of our JRSP scheme is increased by $\mu\sqrt{\bar{\gamma}}(1 - \sqrt{\bar{\gamma}})/3$ in CAD noise channel. This result means that the correlated effect enables to enhance the average fidelity of JRSP which is subject to AD noise.

3 Protecting JRSP by WM and QWR

In Sect. 2, we have studied the influence of CAD noise on JRSP. We find that even though the correlated effect could potentially improve the fidelity, the unfavorable effects of uncorrelated AD noise still remain. In this section, we turn to introduce the technique of WM and QMR to remove the adverse effects in both uncorrelated AD and CAD noises. As mentioned earlier, the state $|\mathcal{G}\rangle_{ABC}$ shared by Alice, Bob and Charlie is subject to a prior WM (carried by Alice) before the qubits suffer the CAD noise; after that a post-QMR is performed by Alice and Bob, respectively. This of operations can be expressed as

$$\rho_{QMR} = M_{QMR} [\varepsilon_{CAD} (M_{WM} \rho M_{WM}^\dagger)] M_{QMR}^\dagger, \tag{21}$$

where M_{WM} and M_{QMR} are non-unitary quantum operations, which are described as follows

$$\begin{aligned} M_{WM} &= \begin{pmatrix} 1 & 0 \\ 0 & \sqrt{1-p} \end{pmatrix}_A \otimes \begin{pmatrix} 1 & 0 \\ 0 & \sqrt{1-p} \end{pmatrix}_B, \\ M_{QWR} &= \begin{pmatrix} \sqrt{1-q} & 0 \\ 0 & 1 \end{pmatrix}_A \otimes \begin{pmatrix} \sqrt{1-q} & 0 \\ 0 & 1 \end{pmatrix}_B. \end{aligned} \tag{22}$$

Here p, q are the measurement strengths of WM and QMR, respectively, and $0 \leq p, q \leq 1$. For $0 < p < 1$, it represents the WM does not completely collapse the state to $|00\rangle$, while $0 < q < 1$ indicates that the measured state is still recoverable. Note that both WM and QMR are local operators, and thus it does not require Alice and Bob in the same place. It is also interesting to find that the QMR could be rewritten as

$$\begin{pmatrix} \sqrt{1-q} & 0 \\ 0 & 1 \end{pmatrix} = \frac{1}{\sqrt{1-q}} X \begin{pmatrix} 1 & 0 \\ 0 & \sqrt{1-q} \end{pmatrix} X, \tag{23}$$

where $X = |0\rangle\langle 1| + |1\rangle\langle 0|$ is bit-flip operation. Equation. (23) means that the QMR is constructed by three local operations: a bit-flip operation, a WM and a second bit-flip operation. The implementation of WM has been achieved in both photonic qubits [1, 2] and superconducting qubits [3]. For instance, as shown in Refs. [1, 2], the WM is implemented with a Brewster angle glass plate (BAGP) for the photon polarization qubit. The BAGP reflects vertical polarization with a certain probability and completely transmits horizontal polarization, which exactly functions as the WM.

From Eqs. (4) and (21), the final state of entangled state can be written as

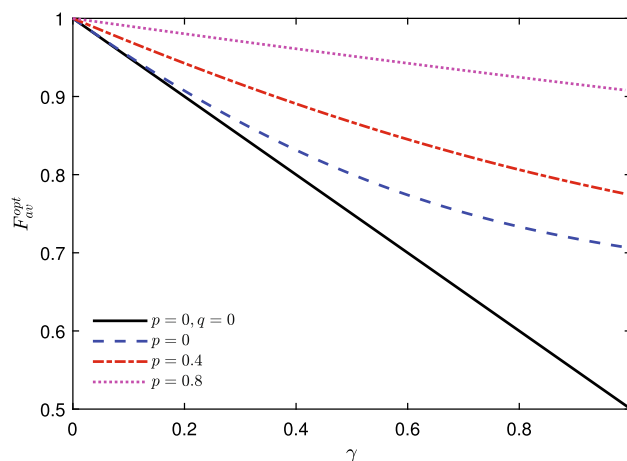
$$\begin{aligned} \rho_{QMR} &= \frac{1}{N} [\bar{q}^2 |000\rangle\langle 000| + V |111\rangle\langle 111| + \bar{q}^2 W |100\rangle\langle 100| \\ &\quad + \bar{q} X (|000\rangle\langle 111| + |111\rangle\langle 000|) + \bar{q} Y (|110\rangle\langle 110| + |101\rangle\langle 101|)], \end{aligned} \tag{24}$$

where $V = \bar{p}^2(\bar{\mu}\bar{\gamma}^2 + \mu\bar{\gamma})$, $W = \bar{p}^2(\bar{\mu}\gamma^2 + \mu\gamma)$, $X = \bar{p}(\bar{\mu}\bar{\gamma} + \mu\sqrt{\bar{\gamma}})$, $Y = \bar{p}^2\bar{\mu}\bar{\gamma}\gamma$. $N = \bar{q}^2(1 + W) + V + 2\bar{q}Y$ is the normalization factor.

Through the standard procedure of JRSP, the state held by Charlie is one of the following four states:

$$\begin{aligned} \rho_0^0(out) = \rho_0^1(out) &= \frac{2}{\sigma_1} \left\{ \left[\bar{q}^2 \cos^2 \frac{\theta}{2} + (\bar{q}^2 W + \bar{q} Y) \sin^2 \frac{\theta}{2} \right] |0\rangle\langle 0| + (V + \bar{q} Y) \sin^2 \frac{\theta}{2} |1\rangle\langle 1| \right. \\ &\quad \left. + \bar{q} X \sin \frac{\theta}{2} \cos \frac{\theta}{2} (e^{-i\phi} |0\rangle\langle 1| + e^{i\phi} |1\rangle\langle 0|) \right\} \\ \rho_1^0(out) = \rho_1^1(out) &= \frac{2}{\sigma_2} \left\{ 2 \left[\bar{q}^2 \sin^2 \frac{\theta}{2} + (\bar{q}^2 W + \bar{q} Y) \cos^2 \frac{\theta}{2} \right] |1\rangle\langle 1| + 2(V + \bar{q} Y) \cos^2 \frac{\theta}{2} |0\rangle\langle 0| \right. \\ &\quad \left. + \bar{q} X \sin \frac{\theta}{2} \cos \frac{\theta}{2} (e^{-i\phi} |0\rangle\langle 1| + e^{i\phi} |1\rangle\langle 0|) \right\} \end{aligned} \tag{25}$$

Fig. 2 Average fidelity F_{av}^{opt} as a function of decoherence strength γ for different measurement strengths p of WM with $\mu = 0$



where $\sigma_1 = (2\bar{q}^2 - N) \cos \theta + N$, $\sigma_2 = (N - 2\bar{q}^2) \cos \theta + N$.

From Eqs. (1), (15), (16) and (25), the state-dependent average fidelity can be obtained as

$$\dot{F}_{av} = \frac{1}{2N} [2(\bar{q}^2 + V + \bar{q}Y) + (\bar{q}^2W + 2\bar{q}X - \bar{q}^2 - V) \sin^2 \theta]. \tag{26}$$

Similarly, we can get the state independent average fidelity

$$\langle \bar{F} \rangle = \frac{(2 + W)\bar{q}^2 + (2X + 3Y)\bar{q} + 2V}{3[(1 + W)\bar{q}^2 + 2Y\bar{q} + V]}. \tag{27}$$

Now, let us make a detailed analysis of the average fidelity $\langle \bar{F} \rangle$. Firstly, in order to achieve the maximal value of $\langle \bar{F} \rangle$, we need to choose the optimal QMR strength q . It can be obtained by calculating the following conditions: $\partial \langle \bar{F} \rangle / \partial q = 0$ and $\partial^2 \langle \bar{F} \rangle / (\partial q)^2 < 0$. Specifically, the following equation holds on here,

$$\partial \langle \bar{F} \rangle / \partial q = \frac{1}{3N} [2\bar{q}(W + 2) + 2X + 3Y] - \frac{2\sigma_3}{3N^2} [\bar{q}(W + 1) + Y] = 0, \tag{28}$$

where $\sigma_3 = \bar{q}^2(2 + W) + \bar{q}(2X + 3Y) + 2V$. Then, from the condition $\partial^2 \langle \bar{F} \rangle / (\partial q)^2 < 0$, the result turns out to be

$$q = 1 + \frac{VW - \sqrt{\sigma_4}}{2X(W + 1) + Y(W - 1)}, \tag{29}$$

where $\sigma_4 = V(VW^2 + 4X^2(W + 1) - Y^2(W - 1) - 4XY)$. Therefore, the maximally teleported average fidelity can be expressed as

$$F_{av}^{opt} = \frac{1}{6} \cdot \frac{4 + 2W + \sigma_5 / \sqrt{\sigma_4}}{1 + W + \sigma_6 / \sqrt{\sigma_4}}, \tag{30}$$

where $\sigma_5 = 4X^2(W + 1) + 3Y^2(W - 1) + 4XY(2W + 1) - 2VW(W + 2)$, $\sigma_6 = Y^2(W - 1) + (2XY - VW)(W + 1)$. Obviously, the teleported average fidelity is equal to 1 when $\gamma = 0$.

Figure 2 shows the result of an average fidelity as a function of decoherence under CAD noise with the assistance of WM and QMR. It is straightforward to note that the average fidelity rapidly decreases with the increase in γ if neither WM nor QWR is executed.

Each line of this figure can be seen as follows.

$$F(p = 0) = - \frac{(\gamma - 1)(4\gamma A_{21} - 32\gamma + 4A_{21} - 3\gamma^2 A_{21} + 8\gamma^3 A_{21} + \gamma^4 A_{21} + 44\gamma^2 - 36\gamma^3 + 18\gamma^4 - 10\gamma^5 + 16)}{3 \left((\gamma - 1)^2 + \frac{(\gamma^2 + 1)(A_{21} - \gamma^2 + \gamma^3)^2}{(\gamma^3 + 2\gamma^2 - \gamma + 2)^2} - \frac{2\gamma(\gamma - 1)(A_{21} - \gamma^2 + \gamma^3)}{\gamma^3 + 2\gamma^2 - \gamma + 2} \right) (\gamma^3 + 2\gamma^2 - \gamma + 2)^2} \tag{31}$$

where $A_{21} = \sqrt{(\gamma - 1)^2 (5\gamma^2 - 4\gamma + 4)}$.

$$F(p = 0.4) = \frac{500\sqrt{5}A_{22} - 16000\gamma + 12300\gamma^2 - 7380\gamma^3 + 1890\gamma^4 - 810\gamma^5 + 300\sqrt{5}\gamma A_{22} - 135\sqrt{5}\gamma^2 A_{22} + 216\sqrt{5}\gamma^3 A_{22} + \frac{81\sqrt{5}\gamma^4 A_{22}}{5} + 10000}{21150\gamma^2 - 24000\gamma - 15390\gamma^3 + 5670\gamma^4 - 2430\gamma^5 + 900\sqrt{5}\gamma A_{22} - 540\sqrt{5}\gamma^2 A_{22} + 324\sqrt{5}\gamma^3 A_{22} + 15000} \tag{32}$$

where $A_{22} = \sqrt{(\gamma - 1)^2 (9\gamma^2 - 12\gamma + 20)}$.

$$F(p = 0.8) = \frac{500\sqrt{5}A_{23} - 12000\gamma + 2700\gamma^2 - 740\gamma^3 + 50\gamma^4 - 10\gamma^5 + 100\sqrt{5}\gamma A_{23} - 15\sqrt{5}\gamma^2 A_{23} + 8\sqrt{5}\gamma^3 A_{23} + \frac{\sqrt{5}\gamma^4 A_{23}}{5} + 10000}{4350\gamma^2 - 18000\gamma - 1470\gamma^3 + 150\gamma^4 - 30\gamma^5 + 300\sqrt{5}\gamma A_{23} - 60\sqrt{5}\gamma^2 A_{23} + 12\sqrt{5}\gamma^3 A_{23} + 15000} \tag{33}$$

where $A_{23} = \sqrt{(\gamma - 1)^2 (\gamma^2 - 4\gamma + 20)}$.

$$F(p = 0, q = 0) = 1 - \frac{\gamma}{2}. \tag{34}$$

However, the average fidelity, when the WM and QMR are introduced, could be enhanced. Particularly, we find the larger the measurement strength of WM is, the larger the average fidelity would be. A more clearer description of the role of p is shown in Fig. 3,

where the plot of F_{av}^{opt} is shown as a function of measurement strength p of WM for different memory parameters μ with $\gamma = 0.5$. Each line of this figure can be expressed as:

$$F(\mu = 0) = \frac{B_{31}^{(0)}}{B_{31}^{(1)}}; F(\mu = 0.4) = \frac{B_{32}^{(0)}}{B_{32}^{(1)}}; F(\mu = 0.8) = \frac{B_{33}^{(0)}}{B_{33}^{(1)}}; F(\mu = 1) = \frac{B_{34}^{(0)}}{B_{34}^{(1)}} \tag{35}$$

where $B_{3i}^{(k)}$ ($i = 1, 2, 3, 4; k = 0, 1$) can be seen in ‘‘Appendix’’.

The participation of WM and QMR enables us to improve the average fidelity on the basis of correlate noise. The maximally achievable fidelity always approaches 1 without regard to γ when $\mu = 0, 1$. However, for the intermediate cases $0 < \mu < 1$, the maximal value of F_{av}^{opt} is less than 1. The explanation of this phenomenon could be understood as follows. From Eq.(3), we note that in both uncorrelated AD and FCAD channels, only one dissipative channel is formulated in the decoherence process, i.e., $|11\rangle \rightarrow (|10\rangle, |01\rangle) \rightarrow |00\rangle$ for uncorrelated AD noise and $|11\rangle \rightarrow |00\rangle$ for FCAD noise. The above features ensure the operation of QMR could recover the initial information before the decoherence. However, for the general CAD channel ($0 < \mu < 1$), the QMR can not exactly distinguish such two dissipative channels, and hence the fidelity cannot achieve 1. To illustrate this phenomenon more clearly, we plot Fig. 4 to show the dependency between the maximal achievable fidelity and the correlated parameter μ . It is obvious that the fidelity is no longer a monotonic function of μ with the given γ and $p > 0$.

Each expression is

$$F(p = 0) = -\frac{B_{41}^{(0)}}{B_{41}^{(1)}}; F(p = 0.5) = -\frac{B_{42}^{(0)}}{B_{42}^{(1)}}; F(p = 0.8) = -\frac{B_{43}^{(0)}}{B_{43}^{(1)}}; F(p = 0.99) = -\frac{B_{44}^{(0)}}{B_{44}^{(1)}}, \tag{36}$$

where $B_{4j}^{(k)}$ can be seen in ‘‘Appendix’’.

Moreover, when no weak measurement operation is implemented from Fig. 4a, it can be concluded that (i) the average fidelity of fully correlated channel ($\mu = 1$) is always greater than general correlated channel ($0 < \mu < 1$), and (ii) the average fidelity of general correlated channel ($0 < \mu < 1$) is always greater than that of uncorrelated channel ($\mu = 0$). However, as long as the measurement strengths of WM, p , is larger than 0, the phenomenon (ii) is not valid. It can be seen from any graph in Fig. 4b–d that when the decoherence strength γ is close to 1, the average fidelity decreases sharply with the small increase in the correlated parameter μ . In combination with Fig. 4b–d, we find that the measurement strength p of WM has an impact on this downward trend, that is, the larger the measurement strength P of WM, the larger the base amount of the average fidelity to be reduced.

Figure 5 shows the average fidelity as a monotonically increasing function of the memory parameter μ with $\gamma = 0.5$, whether WM and QMR are involved or not. Further, we find that for any given memory parameter μ , the greater the measurement strength p of WM is, the greater the average fidelity would be. That is, on the basis of memory enhancing the average fidelity on AD noise, the participation of WM and QWR can further improve the average fidelity of JRSP.

Each expression can be seen as:

$$F(p = 0) = \frac{B_{51}^{(0)}}{B_{51}^{(1)}}; F(p = 0.3) = \frac{B_{52}^{(0)}}{B_{52}^{(1)}}; F(p = 0.5) = \frac{B_{53}^{(0)}}{B_{53}^{(1)}}; F(p = 0.8) = \frac{B_{54}^{(0)}}{B_{54}^{(1)}}, \tag{37}$$

where $B_{5j}^{(k)}$ ($j = 1, 2, 3, 4; k = 0, 1$) can be seen in ‘‘Appendix’’.

Obviously, the total probability of success can be obtained by adding each probability that corresponding to $\rho_j^i(out)$ ($i, j = 0, 1$)

$$p_{total} = \sum_{i,j=0}^1 p_{ij} = \frac{V + W + 2Y - 2q - 2Wq - 2Yq + Wq^2 + q^2 + 1}{N}. \tag{38}$$

where p_{ij} comes from the standard procedure of JRSP. After replacing V, W, Y, N with p, q, μ, γ , the total probability of success can be simplified to 1. Therefore, our scheme is perfect although it suffers noise channel.

4 Conclusion

In summary, by using three-qubit entangled GHZ-state as the quantum channel, we study the influence of correlated AD noise on the scheme of JRSP for arbitrary single-qubit state. Letting the qubits of a sender and the receiver pass through the channel with AD noise, we get results for the JRSP scheme as following: (A) The analytical formulas of the output state in the JRSP scheme under correlated AD noisy channel is presented. Based on these formulae of the output state, the state dependent and independent average fidelities of the target and output states are calculated. Consequently, the expression of the partial derivative of the state independent average fidelity with respect to the correlated parameter μ is obtained. The partial derivative is positive for any value of the decoherence parameter γ , which means that the correlated parameter can increase the fidelity in JRSP in correlated AD noise environment. (B) The state independent average fidelity as a function of the decoherence parameter and the correlated parameter is plotted, and its increment caused by the correlated parameter is given.

Subsequently, utilizing WM and QMR to the uncorrelated and correlated AD noisy channel, we obtain the formulae of the output state in JRSP scheme under AD and CAD noise environments, and calculate the state dependent and independent average fidelities of the target and output states. By making relevant graphics of the state independent average fidelity in JRSP scheme under AD and CAD noise environments, we find that the combined action of WM and QMR can almost completely suppress the AD and CAD decoherence if the careful optimization of the strengths of WM and QMR is carried out. That is, the combination of WM and QMR in both AD and CAD channels can greatly improve the efficiency of JRSP. Our result may be applied to enhance the communication efficiency of experimental realization of JRSP scheme under AD and CAD noise environments.

Acknowledgements This work is supported by 14th Five-Year' Key Discipline of Xinjiang Uygur Autonomous Region, National Science Foundation of Sichuan Province (No. 2022NSFSC0534), the Central Guidance on Local Science and Technology Development Fund of Sichuan Province (No. 22ZYZYTS0064), the Chengdu Key Research and Development Support Program (No. 2021-YF09-0016-GX), the key project of Sichuan Normal University (No. XKZX-02).

Author contributions In fact, all of the authors' contributions to this paper are important. The specific contributions are as follows. The first author played a major role in the conceptualization and writing of the article. The rest authors worked mainly on the overall framework and language of the article.

Data availability The data sets generated during and/or analyzed during the current study are available from the corresponding author on reasonable request.

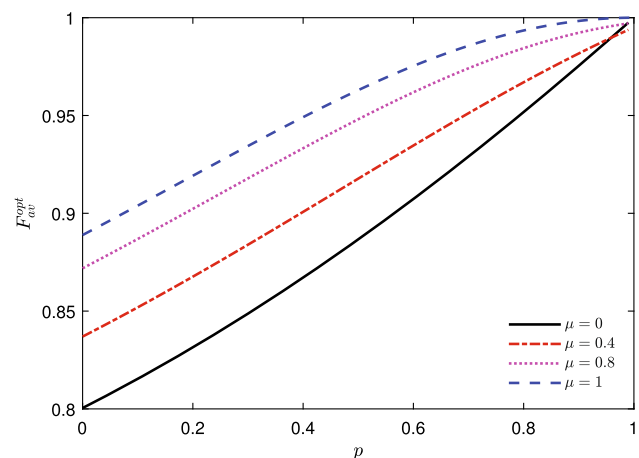
Declarations

Conflict of interest No potential conflict of interest was reported by the authors. All authors of this manuscript have read and approved the final version submitted and contents of this manuscript have not been copyrighted or published previously and is not under consideration for publication elsewhere.

Appendix

This section, we demonstrate the concrete expressions for each line in Figs. 3, 4 and 5.

Fig. 3 Average fidelity F_{av}^{opt} as a function of measurement strength p of WM for different memory parameters μ with $\gamma = 0.5$



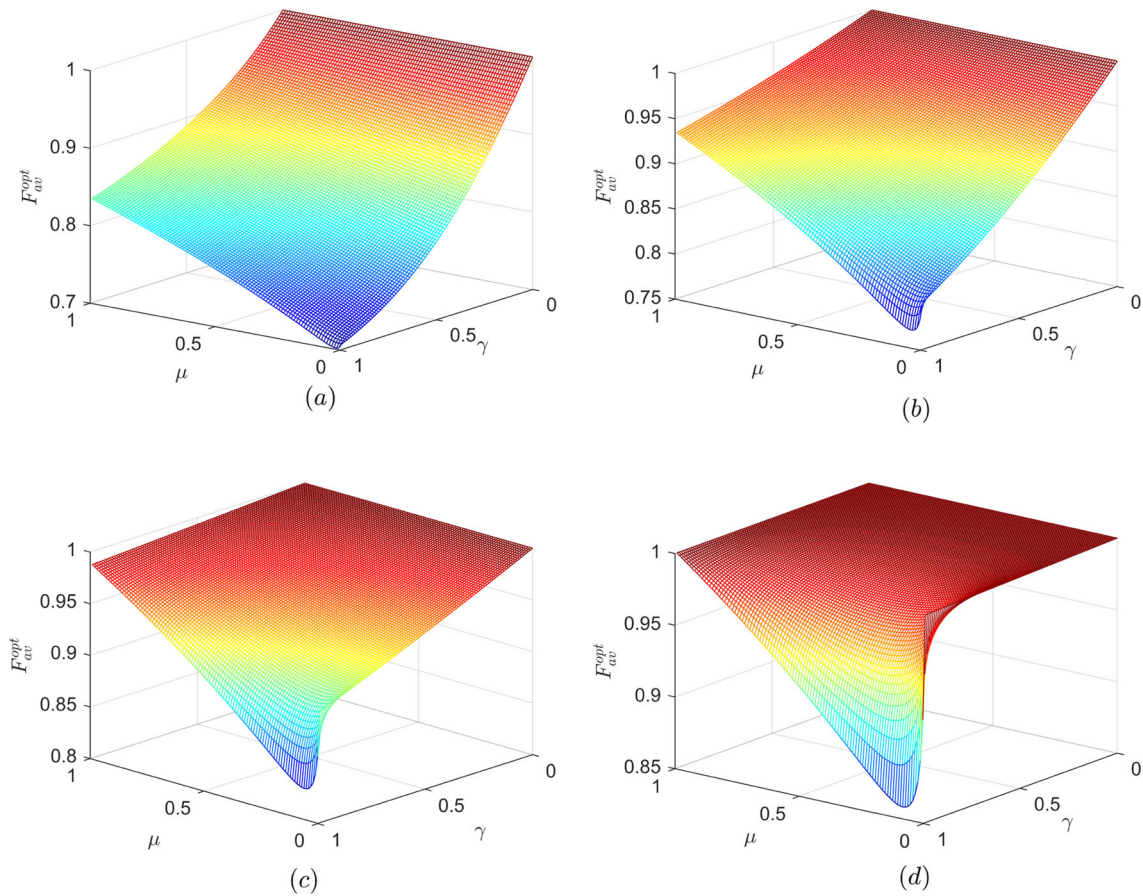
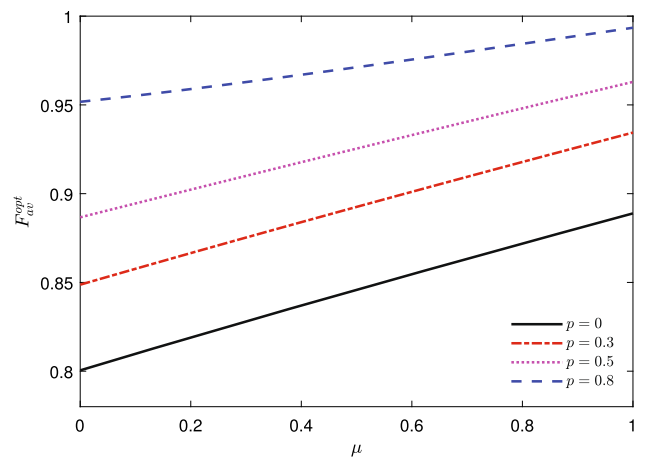


Fig. 4 The relation of γ , μ and F_{av}^{opt} when $p = 0$ in (a), $p = 0.5$ in (b), $p = 0.8$ in (c), $p = 0.99$ in (d)

Fig. 5 Average fidelity F_{av}^{opt} as a function of memory parameter μ for different measurement strength p of WM with $\gamma = 0.5$



Explicit expressions for $B_{3j}^{(k)}$

In Fig. 3, the expressions for each $B_{3j}^{(k)}$ can be seen as follows.

$$B_{21}^{(0)} = 2(p - 1)^2 (101 A_{31} - 60 p A_{31} - 176 p + 248 p^2 - 48 p^3 + 20 p^4 + 42 p^2 A_{31} - 20 p^3 A_{31} + p^4 A_{31} + 468) \tag{39}$$

$$B_{21}^{(1)} = \left(3(p-1)^2 + \frac{48(p-1)^3 \left(\frac{p}{4} + \frac{A_{31}}{4} - \frac{p^2}{8} - \frac{1}{8} \right)}{p^3 - 7p^2 + 7p - 17} + \frac{12(p-1)^2 \left(\frac{p^2}{4} - \frac{p}{2} + \frac{5}{4} \right) (2p + 2A_{31} - p^2 - 1)^2}{(p^3 - 7p^2 + 7p - 17)^2} \right) (p^3 - 7p^2 + 7p - 17)^2 \tag{40}$$

$$B_{32}^{(0)} = 2(p-1)^2 \left(4835\sqrt{7}A_{32} - 982464\sqrt{2}p - 1889664p + 6816\sqrt{14}A_{32} + 1389696\sqrt{2} + 818496\sqrt{2}p^2 - 216384\sqrt{2}p^3 + 65856\sqrt{2}p^4 + 1927296p^2 - 925904p^3 + 386316p^4 - 82320p^5 + 13720p^6 - 2514\sqrt{7}p^2A_{32} + 980\sqrt{7}p^3A_{32} - 497\sqrt{7}p^4A_{32} + 3360\sqrt{14}p^2A_{32} - 672\sqrt{14}p^3A_{32} + 2636\sqrt{7}pA_{32} - 5664\sqrt{14}pA_{32} + 2093756 \right); \tag{41}$$

$$B_{32}^{(1)} = \left(21(p-1)^2 - \frac{3600(p-1)^3 \left(\frac{49p}{100} + \frac{\sqrt{7}A_{32}}{100} - \frac{49p^2}{200} - \frac{49}{200} \right)}{216\sqrt{2} - 112\sqrt{2}p - 171p + 56\sqrt{2}p^2 + 147p^2 - 21p^3 + 285} + \frac{60(p-1)^2 \left(\frac{7p^2}{20} - \frac{7p}{10} + \frac{27}{20} \right) (98p + 2\sqrt{7}A_{32} - 49p^2 - 49)^2}{(216\sqrt{2} - 112\sqrt{2}p - 171p + 56\sqrt{2}p^2 + 147p^2 - 21p^3 + 285)^2} \right) (123120\sqrt{2} - 137712\sqrt{2}p - 194238p + 133728\sqrt{2}p^2 - 61152\sqrt{2}p^3 + 21168\sqrt{2}p^4 - 2352\sqrt{2}p^5 + 186503p^2 - 87332p^3 + 35063p^4 - 6174p^5 + 441p^6 + 174537) \tag{42}$$

where $A_{32} = \sqrt{1056\sqrt{2} - 432\sqrt{2}p - 962p + 336\sqrt{2}p^2 + 941p^2 - 280p^3 + 70p^4 + 1591}$.

$$B_{33}^{(0)} = 2(p-1)^2 \left(14784\sqrt{2}\sqrt{A_{33}} - 1231488\sqrt{2}p - 7982928p + 1354752\sqrt{2} + 26124p\sqrt{A_{33}} + 1026432\sqrt{2}p^2 - 321408\sqrt{2}p^3 + 93312\sqrt{2}p^4 + 22935\sqrt{A_{33}} - 29826p^2\sqrt{A_{33}} + 16740p^3\sqrt{A_{33}} - 4293p^4\sqrt{A_{33}} + 7283592p^2 - 3736368p^3 + 1520532p^4 - 349920p^5 + 58320p^6 + 8640\sqrt{2}p^2\sqrt{A_{33}} - 1728\sqrt{2}p^3\sqrt{A_{33}} - 14016\sqrt{2}p\sqrt{A_{33}} + 7008372 \right) \tag{43}$$

$$B_{33}^{(1)} = \left(27(p-1)^2 - \frac{1200(p-1)^3 \left(\frac{81p}{100} + \frac{3\sqrt{A_{33}}}{100} - \frac{81p^2}{200} - \frac{81}{200} \right)}{464\sqrt{2} - 288\sqrt{2}p - 79p + 144\sqrt{2}p^2 + 63p^2 - 9p^3 + 105} + \frac{540(p-1)^2 \left(\frac{9p^2}{20} - \frac{9p}{10} + \frac{29}{20} \right) (54p + 2\sqrt{A_{33}} - 27p^2 - 27)^2}{(464\sqrt{2} - 288\sqrt{2}p - 79p + 144\sqrt{2}p^2 + 63p^2 - 9p^3 + 105)^2} \right) (97440\sqrt{2} - 133792\sqrt{2}p - 551118p + 134208\sqrt{2}p^2 - 67392\sqrt{2}p^3 + 23328\sqrt{2}p^4 - 2592\sqrt{2}p^5 + 452623p^2 - 177732p^3 + 46863p^4 - 1134p^5 + 81p^6 + 441617) \tag{44}$$

where $A_{33} = 768\sqrt{2} - 416\sqrt{2}p - 3066p + 288\sqrt{2}p^2 + 2273p^2 - 720p^3 + 180p^4 + 3973$.

$$B_{34}^{(0)} = 6p(A_{34})^3 - 750pA_{34} - 13280p + 250A_{34} + 14(A_{34})^3 + 16496p^2 - 13056p^3 + 7648p^4 - 3168p^5 + 976p^6 - 192p^7 + 24p^8 + 955p^2A_{34} - 748p^3A_{34} - 7p^2(A_{34})^3 + 413p^4A_{34} + 4p^3(A_{34})^3 - 158p^5A_{34} - p^4(A_{34})^3 + 45p^6A_{34} - 8p^7A_{34} + p^8A_{34} + 6600 \tag{45}$$

$$B_{34}^{(1)} = 48(p^2 - 2p + 3)^2 A_{34}^2 \tag{46}$$

where $A_{34} = (p^2 - 2p + 5)$

Explicit expressions for $B_{4j}^{(k)}$

In Fig. 4, the expressions for each $B_{4j}^{(k)}$ can be seen as follows. In the upper left figure,

$$B_{41}^{(0)} = 2\mu + 2\gamma + (2\gamma - 2)(\mu\gamma - \gamma + 1) - 2\mu\gamma - 2\mu\sqrt{1 - \gamma} - \gamma(\mu + \gamma - \mu\gamma)$$

$$+ \frac{B_{41}^{(00)}}{B_{41}^{(11)}} - \frac{B_{41}^{(01)}}{B_{41}^{(11)}} + \frac{B_{41}^{(02)}}{B_{41}^{(11)}} - 3\gamma(\mu - 1)(\gamma - 1) + \frac{B_{41}^{(03)}}{B_{41}^{(11)}} - \frac{B_{41}^{(04)}}{B_{41}^{(11)}} + \frac{B_{41}^{(05)}}{B_{41}^{(11)}} - 4 \tag{47}$$

$$B_{41}^{(1)} = \frac{3(\gamma(\mu + \gamma - \mu\gamma) + 1)(\gamma - 1)^2 B_{41}^{(10)2}}{(B_{41}^{(11)})^2} - 3(\gamma - 1)(\mu\gamma - \gamma + 1) + \frac{6\gamma(\mu - 1)(\gamma - 1)^2 B_{41}^{(10)}}{B_{41}^{(11)}} \tag{48}$$

where

$$B_{41}^{(00)} = 16\mu^2\gamma^2 - 12\gamma - 8\mu - 8\mu^2\gamma^3 + 4\gamma\sqrt{A_{41}^{(0)}} + 24\mu\gamma - 4\sqrt{A_{41}^{(0)}} + 8\mu\sqrt{1-\gamma} - 36\mu\gamma^2 - 8\mu^2\gamma + 20\mu\gamma^3 + 16\gamma^2 - 12\gamma^3 + 8\mu\gamma^2\sqrt{1-\gamma} + 8\mu^2\gamma\sqrt{1-\gamma} - 8\mu^2\gamma^2\sqrt{1-\gamma} + 8 \tag{49}$$

$$B_{41}^{(01)} = 2(A_{41}^{(1)})^2 \tag{50}$$

$$B_{41}^{(02)} = (2\mu\gamma - 2\gamma - 2\mu + 2\mu\sqrt{1-\gamma} + 2)(A_{41}^{(1)}) \tag{51}$$

$$B_{41}^{(03)} = 2\gamma(\mu + \gamma - \mu\gamma)(A_{41}^{(1)}) \tag{52}$$

$$B_{41}^{(04)} = \gamma(\mu + \gamma - \mu\gamma)(A_{41}^{(1)})^2 \tag{53}$$

$$B_{41}^{(05)} = 3\gamma(\mu - 1)(\gamma - 1)(A_{41}^{(1)}) \tag{54}$$

$$B_{41}^{(10)} = \left(\mu^2\gamma^2 - \mu^2\gamma^3 + \mu\gamma - A_{41}^{(\frac{1}{2})} - 2\mu\gamma^2 + 2\mu\gamma^3 + \gamma^2 - \gamma^3\right) \tag{55}$$

$$B_{41}^{(11)} = 3\mu^2\gamma^2 - 3\gamma - 2\mu - \mu^2\gamma^4 + 5\mu\gamma + 2\mu\sqrt{1-\gamma} - 6\mu\gamma^2 - 2\mu^2\gamma + \mu\gamma^3 + 2\mu\gamma^4 + 3\gamma^2 - \gamma^3 - \gamma^4 + 2\mu\gamma^2\sqrt{1-\gamma} + 2\mu^2\gamma\sqrt{1-\gamma} - 2\mu^2\gamma^2\sqrt{1-\gamma} + 2 \tag{56}$$

$$A_{41}^{(0)} = (\mu\gamma - \gamma + 1)\left(30\mu^2\gamma^2 - 8\gamma - 8\mu - 14\mu^2\gamma^3 - 12\mu^3\gamma^2 + 4\mu^3\gamma^3 + 20\mu\gamma + 8\mu\sqrt{1-\gamma} - 26\mu\gamma^2 - 16\mu^2\gamma + 15\mu\gamma^3 + 8\mu^3\gamma - 8\mu^2\sqrt{1-\gamma} + 8\mu^2 + 9\gamma^2 - 5\gamma^3 + 8\mu\gamma^2\sqrt{1-\gamma} + 12\mu^2\gamma\sqrt{1-\gamma} - 8\mu^3\gamma\sqrt{1-\gamma} - 16\mu^2\gamma^2\sqrt{1-\gamma} + 8\mu^3\gamma^2\sqrt{1-\gamma} - 4\mu\gamma\sqrt{1-\gamma} + 4\right) \tag{57}$$

$$A_{41}^{(1)} = 4\mu^2\gamma^2 - 3\gamma - 2\mu - 2\mu^2\gamma^3 + \gamma\sqrt{A_{41}^{(0)}} + 6\mu\gamma - \sqrt{A_{41}^{(0)}} + 2\mu\sqrt{1-\gamma} - 9\mu\gamma^2 - 2\mu^2\gamma + 5\mu\gamma^3 + 4\gamma^2 - 3\gamma^3 + 2\mu\gamma^2\sqrt{1-\gamma} + 2\mu^2\gamma\sqrt{1-\gamma} - 2\mu^2\gamma^2\sqrt{1-\gamma} + 2 \tag{58}$$

In the upper right figure,

$$B_{42}^{(0)} = \frac{B_{42}^{(00)}}{B_{42}^{(11)}} - 4\gamma - 4\mu + 4\mu\gamma + 4\mu\sqrt{1-\gamma} + \gamma(\mu + \gamma - \mu\gamma) + \frac{B_{42}^{(01)}}{(B_{42}^{(11)})^2} - 2(\gamma - 1)(\mu\gamma - \gamma + 1) + 3\gamma(\mu - 1)(\gamma - 1) + \frac{B_{42}^{(02)}}{B_{42}^{(11)}} + \frac{B_{42}^{(03)}}{B_{42}^{(11)}} + \frac{B_{42}^{(04)}}{(B_{42}^{(11)})^2} + \frac{B_{42}^{(05)}}{B_{42}^{(11)}} + 12 \tag{59}$$

$$B_{42}^{(1)} = 3(\gamma - 1)(\mu\gamma - \gamma + 1) - \frac{12(\gamma - 1)^2\left(\frac{\mu\gamma}{4} - \frac{\mu\gamma^2}{4} + \frac{\gamma^2}{4} + 1\right)(B_{42}^{(10)})^2}{(B_{42}^{(11)})^2} + \frac{6\gamma(\mu - 1)(\gamma - 1)^2 B_{42}^{(10)}}{B_{42}^{(11)}} \tag{60}$$

where

$$B_{42}^{(00)} = 4\left(32\mu^2\gamma^2 - 80\gamma - 64\mu - 16\mu^2\gamma^3 + 4\gamma\sqrt{A_{42}^{(0)}} + 100\mu\gamma - 4\sqrt{A_{42}^{(0)}} + 64\mu\sqrt{1-\gamma} - 72\mu\gamma^2 - 16\mu^2\gamma + 36\mu\gamma^3 + 36\gamma^2 - 20\gamma^3 + 16\mu\gamma^2\sqrt{1-\gamma} + 16\mu^2\gamma\sqrt{1-\gamma} - 16\mu^2\gamma^2\sqrt{1-\gamma} + 64\right) \tag{61}$$

$$B_{42}^{(01)} = 8\left(8\mu^2\gamma^2 - 20\gamma - 16\mu - 4\mu^2\gamma^3 + \gamma\sqrt{A_{42}^{(0)}} + 25\mu\gamma - \sqrt{A_{42}^{(0)}} + 16\mu\sqrt{1-\gamma} - 18\mu\gamma^2 - 4\mu^2\gamma + 9\mu\gamma^3 + 9\gamma^2 - 5\gamma^3 + 4\mu\gamma^2\sqrt{1-\gamma} + 4\mu^2\gamma\sqrt{1-\gamma} - 4\mu^2\gamma^2\sqrt{1-\gamma} + 16\right)^2 \tag{62}$$

$$B_{42}^{(02)} = 4(8\mu\gamma - 8\gamma - 8\mu + 8\mu\sqrt{1-\gamma} + 8)(A_{42}^{(1)}) \tag{63}$$

$$B_{42}^{(03)} = 16\gamma(\mu + \gamma - \mu\gamma)(A_{42}^{(1)}) \tag{64}$$

$$B_{42}^{(04)} = \gamma(\mu + \gamma - \mu\gamma) \left(8\mu^2\gamma^2 - 20\gamma - 16\mu - 4\mu^2\gamma^3 + \gamma\sqrt{A_{42}^{(0)}} + 25\mu\gamma - \sqrt{A_{42}^{(0)}} + 16\mu\sqrt{1-\gamma} - 18\mu\gamma^2 - 4\mu^2\gamma + 9\mu\gamma^3 + 9\gamma^2 - 5\gamma^3 + 4\mu\gamma^2\sqrt{1-\gamma} + 4\mu^2\gamma\sqrt{1-\gamma} - 4\mu^2\gamma^2\sqrt{1-\gamma} + 16 \right)^2 \tag{65}$$

$$B_{42}^{(05)} = 24\gamma(\mu - 1)(\gamma - 1) \left(A_{42}^{(1)} \right) \tag{66}$$

$$B_{42}^{(10)} = \left(\mu^2\gamma^2 - \mu^2\gamma^3 + \mu\gamma - \sqrt{A_{42}^{(0)}} - 2\mu\gamma^2 + 2\mu\gamma^3 + \gamma^2 - \gamma^3 \right) \tag{67}$$

$$B_{42}^{(11)} = 16\mu + 20\gamma - 7\mu^2\gamma^2 + 2\mu^2\gamma^3 + \mu^2\gamma^4 - 24\mu\gamma - 16\mu\sqrt{1-\gamma} + 15\mu\gamma^2 + 4\mu^2\gamma - 5\mu\gamma^3 - 2\mu\gamma^4 - 8\gamma^2 + 3\gamma^3 + \gamma^4 - 4\mu\gamma^2\sqrt{1-\gamma} - 4\mu^2\gamma\sqrt{1-\gamma} + 4\mu^2\gamma^2\sqrt{1-\gamma} - 16 \tag{68}$$

$$A_{42}^{(0)} = (\mu\gamma - \gamma + 1) \left(133\mu^2\gamma^2 - 96\gamma - 128\mu - 53\mu^2\gamma^3 - 48\mu^3\gamma^2 + 16\mu^3\gamma^3 + 208\mu\gamma + 128\mu\sqrt{1-\gamma} - 136\mu\gamma^2 - 128\mu^2\gamma + 57\mu\gamma^3 + 32\mu^3\gamma - 128\mu^2\sqrt{1-\gamma} + 128\mu^2 + 52\gamma^2 - 20\gamma^3 + 32\mu\gamma^2\sqrt{1-\gamma} + 64\mu^2\gamma\sqrt{1-\gamma} - 32\mu^3\gamma\sqrt{1-\gamma} - 64\mu^2\gamma^2\sqrt{1-\gamma} + 32\mu^3\gamma^2\sqrt{1-\gamma} - 32\mu\gamma\sqrt{1-\gamma} + 64 \right) \tag{69}$$

$$A_{42}^{(1)} = \mu^2\gamma^2 - \frac{5\gamma}{2} - 2\mu - \frac{\mu^2\gamma^3}{2} + \frac{\gamma\sqrt{A_{42}^{(0)}}}{8} + \frac{25\mu\gamma}{8} - \frac{\sqrt{A_{42}^{(0)}}}{8} + 2\mu\sqrt{1-\gamma} - \frac{9\mu\gamma^2}{4} - \frac{\mu^2\gamma}{2} + \frac{9\mu\gamma^3}{8} + \frac{9\gamma^2}{8} - \frac{5\gamma^3}{8} + \frac{\mu\gamma^2\sqrt{1-\gamma}}{2} + \frac{\mu^2\gamma\sqrt{1-\gamma}}{2} - \frac{\mu^2\gamma^2\sqrt{1-\gamma}}{2} + 2 \tag{70}$$

In the bottom left figure,

$$B_{43}^{(0)} = \frac{B_{43}^{(00)}}{B_{43}^{(11)}} - 10\gamma - (2\gamma - 2)(\mu\gamma - \gamma + 1) - 10\mu + 10\mu\gamma + 10\mu\sqrt{1-\gamma} + \gamma(\mu + \gamma - \mu\gamma) + \frac{2B_{43}^{(00)}}{\left(B_{43}^{(11)} \right)^2} + 3\gamma(\mu - 1)(\gamma - 1) + \frac{B_{43}^{(01)}}{B_{43}^{(11)}} + \frac{B_{43}^{(02)}}{B_{43}^{(11)}} + \frac{B_{43}^{(03)}}{\left(B_{43}^{(11)} \right)^2} + \frac{B_{43}^{(04)}}{B_{43}^{(11)}} + 60 \tag{71}$$

$$B_{43}^{(1)} = 3(\gamma - 1)(\mu\gamma - \gamma + 1) - \frac{75(\gamma - 1)^2 \left(\frac{\mu\gamma}{25} - \frac{\mu\gamma^2}{25} + \frac{\gamma^2}{25} + 1 \right) \left(B_{43}^{(10)} \right)^2}{\left(B_{43}^{(11)} \right)^2} + \frac{6\gamma(\mu - 1)(\gamma - 1)^2 B_{43}^{(10)}}{B_{43}^{(11)}} \tag{72}$$

$$B_{43}^{(00)} = 25 \left(20\mu^2\gamma^2 - 275\gamma - 250\mu - 10\mu^2\gamma^3 + \gamma\sqrt{A_{43}^{(0)}} + 286\mu\gamma - \sqrt{A_{43}^{(0)}} + 250\mu\sqrt{1-\gamma} - 57\mu\gamma^2 - 10\mu^2\gamma + 21\mu\gamma^3 + 36\gamma^2 - 11\gamma^3 + 10\mu\gamma^2\sqrt{1-\gamma} + 10\mu^2\gamma\sqrt{1-\gamma} - 10\mu^2\gamma^2\sqrt{1-\gamma} + 250 \right)^2 \tag{73}$$

$$B_{43}^{(01)} = 25 \left(50\mu\gamma - 50\gamma - 50\mu + 50\mu\sqrt{1-\gamma} + 50 \right) \left(A_{43}^{(1)} \right) \tag{74}$$

$$B_{43}^{(02)} = 250\gamma(\mu + \gamma - \mu\gamma) \left(A_{43}^{(1)} \right) \tag{75}$$

$$B_{43}^{(03)} = \gamma(\mu + \gamma - \mu\gamma) \left(20\mu^2\gamma^2 - 275\gamma - 250\mu - 10\mu^2\gamma^3 + \gamma\sqrt{A_{43}^{(0)}} + 286\mu\gamma - \sqrt{A_{43}^{(0)}} + 250\mu\sqrt{1-\gamma} - 57\mu\gamma^2 - 10\mu^2\gamma + 21\mu\gamma^3 + 36\gamma^2 - 11\gamma^3 + 10\mu\gamma^2\sqrt{1-\gamma} + 10\mu^2\gamma\sqrt{1-\gamma} - 10\mu^2\gamma^2\sqrt{1-\gamma} + 250 \right)^2 \tag{76}$$

$$B_{43}^{(04)} = 375\gamma(\mu - 1)(\gamma - 1) \left(A_{43}^{(1)} \right) \tag{77}$$

$$B_{43}^{(10)} = \left(\mu^2\gamma^2 - \mu^2\gamma^3 + \mu\gamma - \sqrt{A_{43}^{(0)}} - 2\mu\gamma^2 + 2\mu\gamma^3 + \gamma^2 - \gamma^3 \right) \tag{78}$$

$$B_{43}^{(11)} = 250\mu + 275\gamma - 19\mu^2\gamma^2 + 8\mu^2\gamma^3 + \mu^2\gamma^4 - 285\mu\gamma - 250\mu\sqrt{1-\gamma} + 54\mu\gamma^2 + 10\mu^2\gamma - 17\mu\gamma^3 - 2\mu\gamma^4 - 35\gamma^2 + 9\gamma^3 + \gamma^4 - 10\mu\gamma^2\sqrt{1-\gamma} - 10\mu^2\gamma\sqrt{1-\gamma} + 10\mu^2\gamma^2\sqrt{1-\gamma} - 250 \tag{79}$$

$$A_{43}^{(0)} = (\mu\gamma - \gamma + 1) \left(1126\mu^2\gamma^2 - 3000\gamma - 5000\mu - 326\mu^2\gamma^3 - 300\mu^3\gamma^2 + 100\mu^3\gamma^3 + 6100\mu\gamma + 5000\mu\sqrt{1-\gamma} - 1450\mu\gamma^2 - 3200\mu^2\gamma + 351\mu\gamma^3 + 200\mu^3\gamma - 5000\mu^2\sqrt{1-\gamma} + 5000\mu^2 + 625\gamma^2 - 125\gamma^3 + 200\mu\gamma^2\sqrt{1-\gamma} + 700\mu^2\gamma\sqrt{1-\gamma} - 200\mu^3\gamma\sqrt{1-\gamma} - 400\mu^2\gamma^2\sqrt{1-\gamma} + 200\mu^3\gamma^2\sqrt{1-\gamma} - 500\mu\gamma\sqrt{1-\gamma} + 2500 \right) \tag{80}$$

$$A_{43}^{(1)} = \frac{4\mu^2\gamma^2}{25} - \frac{11\gamma}{5} - 2\mu - \frac{2\mu^2\gamma^3}{25} + \frac{\gamma\sqrt{A_{43}^{(0)}}}{125} + \frac{286\mu\gamma}{125} - \frac{\sqrt{A_{43}^{(0)}}}{125} + 2\mu\sqrt{1-\gamma} - \frac{57\mu\gamma^2}{125} - \frac{2\mu^2\gamma}{25} + \frac{21\mu\gamma^3}{125} + \frac{36\gamma^2}{125} - \frac{11\gamma^3}{125} + \frac{2\mu\gamma^2\sqrt{1-\gamma}}{25} + \frac{2\mu^2\gamma\sqrt{1-\gamma}}{25} - \frac{2\mu^2\gamma^2\sqrt{1-\gamma}}{25} + 2 \tag{81}$$

In the bottom right figure,

$$B_{44}^{(0)} = \frac{B_{44}^{(00)}}{(B_{44}^{(11)})^2} - 200\gamma - 200\mu + 200\mu\gamma + 200\mu\sqrt{1-\gamma} + \gamma(\mu + \gamma - \mu\gamma) + \frac{2B_{44}^{(00)}}{B_{44}^{(11)}} - 2(\gamma - 1)(\mu\gamma - \gamma + 1) + \frac{B_{44}^{(01)}}{B_{44}^{(11)}} + 3\gamma(\mu - 1)(\gamma - 1) + \frac{B_{44}^{(02)}}{(B_{44}^{(11)})^2} + \frac{B_{44}^{(03)}}{B_{44}^{(11)}} + \frac{B_{44}^{(04)}}{B_{44}^{(11)}} + 20200 \tag{82}$$

$$B_{44}^1 = 3(\gamma - 1)(\mu\gamma - \gamma + 1) - \frac{3(\gamma - 1)^2(\mu\gamma - \mu\gamma^2 + \gamma^2 + 10000)(B_{44}^{(10)})^2}{(B_{44}^{(11)})^2} + \frac{6\gamma(\mu - 1)(\gamma - 1)^2 B_{44}^{(10)}}{B_{44}^{(11)}} \tag{83}$$

$$B_{44}^{(00)} = 20000 \left(400\mu^2\gamma^2 - 2010000\gamma - 2000000\mu - 200\mu^2\gamma^3 + 2010201\mu\gamma + \gamma\sqrt{(\mu\gamma - \gamma + 1)(A_{44}^{(0)})} + 2000000\mu\sqrt{1-\gamma} - \sqrt{(\mu\gamma - \gamma + 1)(A_{44}^{(0)})} - 10602\mu\gamma^2 - 200\mu^2\gamma + 401\mu\gamma^3 + 10201\gamma^2 - 201\gamma^3 + 200\mu\gamma^2\sqrt{1-\gamma} + 200\mu^2\gamma\sqrt{1-\gamma} - 200\mu^2\gamma^2\sqrt{1-\gamma} + 2000000 \right)^2 \tag{84}$$

$$B_{44}^{(01)} = 10000 \left(20000\mu\gamma - 20000\gamma - 20000\mu + 20000\mu\sqrt{1-\gamma} + 20000 \right) (A_{44}^{(1)}) \tag{85}$$

$$B_{44}^{(02)} = \gamma(\mu + \gamma - \mu\gamma) \left(400\mu^2\gamma^2 - 2010000\gamma - 2000000\mu - 200\mu^2\gamma^3 + 2010201\mu\gamma + \gamma\sqrt{(\mu\gamma - \gamma + 1)(A_{44}^{(0)})} + 2000000\mu\sqrt{1-\gamma} - \sqrt{(\mu\gamma - \gamma + 1)(A_{44}^{(0)})} - 10602\mu\gamma^2 - 200\mu^2\gamma + 401\mu\gamma^3 + 10201\gamma^2 - 201\gamma^3 + 200\mu\gamma^2\sqrt{1-\gamma} + 200\mu^2\gamma\sqrt{1-\gamma} - 200\mu^2\gamma^2\sqrt{1-\gamma} + 2000000 \right)^2 \tag{86}$$

$$B_{44}^{(03)} = 2000000\gamma(\mu + \gamma - \mu\gamma) (A_{44}^{(1)}) \tag{87}$$

$$B_{44}^{(04)} = 3000000\gamma(\mu - 1)(\gamma - 1) (A_{44}^{(1)}) \tag{88}$$

$$B_{44}^{(10)} = \left(\mu^2\gamma^2 - \mu^2\gamma^3 + \mu\gamma - \sqrt{(\mu\gamma - \gamma + 1)(A_{44}^{(0)})} - 2\mu\gamma^2 + 2\mu\gamma^3 + \gamma^2 - \gamma^3 \right) \tag{89}$$

$$B_{44}^{(11)} = 2000000\mu + 2010000\gamma - 399\mu^2\gamma^2 + 198\mu^2\gamma^3 + \mu^2\gamma^4 - 2010200\mu\gamma - 2000000\mu\sqrt{1-\gamma} + 10599\mu\gamma^2 + 200\mu^2\gamma - 397\mu\gamma^3 - 2\mu\gamma^4 - 10200\gamma^2 + 199\gamma^3 + \gamma^4 - 200\mu\gamma^2\sqrt{1-\gamma} - 200\mu^2\gamma\sqrt{1-\gamma} + 200\mu^2\gamma^2\sqrt{1-\gamma} - 2000000 \tag{90}$$

$$A_{44}^{(0)} = 4250001\mu^2\gamma^2 - 404000000\gamma - 800000000\mu - 130001\mu^2\gamma^3 - 120000\mu^3\gamma^2 + 40000\mu^3\gamma^3 + 808040000\mu\gamma + 800000000\mu\sqrt{1-\gamma} - 8180000\mu\gamma^2 - 404080000\mu^2\gamma + 140001\mu\gamma^3 + 80000\mu^3\gamma - 800000000\mu^2\sqrt{1-\gamma} + 800000000\mu^2 + 4050000\gamma^2 - 50000\gamma^3 + 80000\mu\gamma^2\sqrt{1-\gamma} + 4080000\mu^2\gamma\sqrt{1-\gamma} - 80000\mu^3\gamma\sqrt{1-\gamma} - 160000\mu^2\gamma^2\sqrt{1-\gamma} + 80000\mu^3\gamma^2\sqrt{1-\gamma} - 4000000\mu\gamma\sqrt{1-\gamma} + 400000000 \tag{91}$$

$$A_{44}^{(1)} = \frac{\mu^2\gamma^2}{2500} - \frac{201\gamma}{100} - 2\mu - \frac{\mu^2\gamma^3}{5000} + \frac{2010201\mu\gamma}{1000000} + \frac{\gamma\sqrt{(\mu\gamma - \gamma + 1)(A_{44}^{(0)})}}{1000000} + 2\mu\sqrt{1-\gamma} - \frac{\sqrt{(\mu\gamma - \gamma + 1)(A_{44}^{(0)})}}{1000000} - \frac{5301\mu\gamma^2}{500000} - \frac{\mu^2\gamma}{5000} + \frac{401\mu\gamma^3}{1000000}$$

$$+ \frac{10201\gamma^2}{1000000} - \frac{201\gamma^3}{1000000} + \frac{\mu\gamma^2\sqrt{1-\gamma}}{5000} + \frac{\mu^2\gamma\sqrt{1-\gamma}}{5000} - \frac{\mu^2\gamma^2\sqrt{1-\gamma}}{5000} + 2 \tag{92}$$

Explicit expressions for $B_{5j}^{(k)}$

In Fig. 5, the expressions for each $B_{5j}^{(k)}$ can be seen as follows.

$$B_{51}^{(0)} = 2304\sqrt{2}\mu - 472\mu - 482\mu A_{51} + 202 A_{51} + 832\sqrt{2}\mu^2 - 2240\sqrt{2}\mu^3 - 832\sqrt{2}\mu^4 - 64\sqrt{2}\mu^5 + 374\mu^2 A_{51} + 130\mu^3 A_{51} + 1736\mu^2 + 4376\mu^3 + 1328\mu^4 + 96\mu^5 - 320\sqrt{2}\mu^2 A_{51} - 96\sqrt{2}\mu^3 A_{51} + 416\sqrt{2}\mu A_{51} + 936 \tag{93}$$

$$B_{51}^{(1)} = \left(3\mu + \frac{3(\mu + 5)(2\mu - 2A_{51} + \mu^2 + 1)^2}{(20\sqrt{2}\mu - 12\mu + 4\sqrt{2}\mu^2 - 5\mu^2 + 17)^2} + \frac{3(16\mu - 16)\left(\frac{\mu}{4} - \frac{A_{51}}{4} + \frac{\mu^2}{8} + \frac{1}{8}\right)}{20\sqrt{2}\mu - 12\mu + 4\sqrt{2}\mu^2 - 5\mu^2 + 17} \right) + 3(680\sqrt{2}\mu - 408\mu - 344\sqrt{2}\mu^2 - 296\sqrt{2}\mu^3 - 40\sqrt{2}\mu^4 + 774\mu^2 + 440\mu^3 + 57\mu^4 + 289) \tag{94}$$

where $A_{51} = \sqrt{(\mu + 1)(32\sqrt{2}\mu - 21\mu - 24\sqrt{2}\mu^2 - 8\sqrt{2}\mu^3 + 46\mu^2 + 12\mu^3 + 13)}$.

$$B_{52}^{(0)} = 100907385600\sqrt{2}\mu - 32975491192\mu - 188364722\mu\sqrt{(\mu + 1)A_{52}} + 84523138\sqrt{(\mu + 1)A_{52}} + 18869939200\sqrt{2}\mu^2 - 100154432000\sqrt{2}\mu^3 - 18869939200\sqrt{2}\mu^4 - 752953600\sqrt{2}\mu^5 + 196853678\mu^2\sqrt{(\mu + 1)A_{52}} + 28663138\mu^3\sqrt{(\mu + 1)A_{52}} + 69808280024\mu^2 + 173779616024\mu^3 + 29359447208\mu^4 + 1129430400\mu^5 - 147392000\sqrt{2}\mu^2\sqrt{(\mu + 1)A_{52}} - 20744640\sqrt{2}\mu^3\sqrt{(\mu + 1)A_{52}} + 168136640\sqrt{2}\mu\sqrt{(\mu + 1)A_{52}} + 42765828000 \tag{95}$$

$$B_{52}^{(1)} = \left(147\mu + 3(548800\mu - 548800)\left(\frac{49\mu}{400} - \frac{\sqrt{(\mu + 1)A_{52}}}{400} + \frac{49\mu^2}{800} + \frac{49}{800}\right) \frac{1}{B_{52}^{(10)}} \right) + 3(2401\mu + 22001)\left(98\mu - 2\sqrt{(\mu + 1)A_{52}} + 49\mu^2 + 49\right)^2 \frac{1}{(B_{52}^{(10)})^2} + 147(556867760\sqrt{2}\mu - 409279200\mu - 413372240\sqrt{2}\mu^2 - 134467760\sqrt{2}\mu^3 - 9027760\sqrt{2}\mu^4 + 747956382\mu^2 + 201605600\mu^3 + 12987009\mu^4 + 240343009) \tag{96}$$

$$B_{52}^{(10)} = 17960\sqrt{2}\mu - 13200\mu + 1960\sqrt{2}\mu^2 - 2303\mu^2 + 15503 \tag{97}$$

where $A_{52} = (303200\sqrt{2}\mu - 234999\mu - 264000\sqrt{2}\mu^2 - 39200\sqrt{2}\mu^3 + 450901\mu^2 + 58800\mu^3 + 128500)$.

$$B_{53}^{(0)} = \frac{4447014038798929\mu}{34359738368} + \frac{1731999573283827\mu A_{53}}{1099511627776} + 2530 A_{53} - 256\sqrt{2}\mu^5 - \frac{42546806858567\mu^2 A_{53}}{1099511627776} + 450\mu^3 A_{53} + \frac{13712264631662189\mu^2}{137438953472} + \frac{954132002979149\mu^3}{34359738368} + \frac{203154529470867\mu^4}{137438953472} + 384\mu^5 - 320\sqrt{2}\mu^3 A_{53} + 55968 \tag{98}$$

$$B_{53}^{(1)} = \left(3\mu + \frac{3(64\mu - 64)\left(\frac{\mu}{16} - \frac{A_{53}}{16} + \frac{\mu^2}{32} + \frac{1}{32}\right)}{B_{53}^{(10)}} + \frac{3(\mu + 17)(2\mu - 2A_{53} + \mu^2 + 1)^2}{(B_{53}^{(10)})^2} \right) + 3\left(\frac{166993454639279\mu}{8589934592} - 144\sqrt{2}\mu^4 + \frac{60243921354669\mu^2}{8589934592} + \frac{408726400289561\mu^3}{1099511627776} + 209\mu^4 + 14641\right) \tag{99}$$

$$B_{53}^{(10)} = 136\sqrt{2}\mu - 112\mu + 8\sqrt{2}\mu^2 - 9\mu^2 + 121 \tag{100}$$

where $A_{53} = \sqrt{(\mu + 1)\left(\frac{149436005184641\mu}{549755813888} - 32\sqrt{2}\mu^3 + \frac{804247227640749\mu^2}{8796093022208} + 48\mu^3 + 212\right)}$.

$$B_{54}^{(0)} = \frac{1961207684361405\mu}{67108864} + \frac{538579401443961\mu A_{54}}{8589934592} + 87562 A_{54}$$

$$\begin{aligned}
 &+ \frac{165512947439037 \mu^2 A_{54}}{17179869184} + \frac{40123449911847 \mu^3 A_{54}}{549755813888} + \frac{39193419728658571 \mu^2}{2147483648} \\
 &+ \frac{125668827204021 \mu^3}{33554432} + \frac{98298304814965 \mu^4}{2147483648} + \frac{37729274270505 \mu^5}{274877906944} + 14673000 \tag{101}
 \end{aligned}$$

$$\begin{aligned}
 B_{54}^{(1)} = & \left(3 \mu + \frac{3(400 \mu - 400) \left(\frac{\mu}{100} - \frac{A_{54}}{100} + \frac{\mu^2}{200} + \frac{1}{200} \right)}{B_{54}^{(10)}} + \frac{3(\mu + 101)(2\mu - 2A_{54} + \mu^2 + 1)^2}{(B_{54}^{(10)})^2} \right. \\
 & + 3) \left(\frac{116681510080633 \mu^4}{2199023255552} + \frac{239451137688417 \mu^3}{17179869184} + \frac{126605283049529 \mu^2}{134217728} \right. \\
 & \left. \left. + \frac{493342114160233 \mu}{134217728} + 3690241 \right) \tag{102}
 \end{aligned}$$

$$B_{54}^{(10)} = \frac{525957652160415 \mu}{549755813888} + 20 \sqrt{2} \mu^2 - 21 \mu^2 + 1921 \tag{103}$$

where $A_{54} = \sqrt{(\mu + 1) \left(\frac{618743323903621 \mu}{68719476736} - 200 \sqrt{2} \mu^3 + \frac{620108701709191 \mu^2}{274877906944} + 300 \mu^3 + 9125 \right)}$.

References

1. H. Abulkasim, S. Hamad, K.E. Bahnasy et al., Authenticated quantum secret sharing with quantum dialogue based on Bell states. *Phys. Scr.* **91**, 085101 (2016)
2. J.A. Bergou, M. Hillery, A quantum controlled quantum eraser. *Phys. Scr.* **93**, 124007 (2018)
3. Z. Li, H. Zuo, A novel quantum broadcasting multiparty blind signature scheme. *Phys. Scr.* **93**, 095102 (2018)
4. M.S. Kang, Y.H. Choi, Y. Kim et al., Quantum message authentication scheme based on remote state preparation. *Phys. Scr.* **93**, 115102 (2018)
5. Q. Dong, A.A.S. Manilla, I.L. Yáñez et al., Tetrapartite entanglement measures of GHZ state with uniform acceleration. *Phys. Scr.* **94**, 105101 (2019)
6. S. Shahsavari, M. Motamedifar, H. Safari, Exact dynamics of concurrence-based entanglement in a system of four spin-1/2 particles on a triangular ladder structure. *Phys. Scr.* **95**, 015102 (2020)
7. E.B. Karlsson, Quantum entanglement in low-energy neutron–proton scattering and its possible consequences. *Phys. Scr.* **95**, 025003 (2020)
8. C.H. Bennet, G. Brassard, C. Crépeau, R. Jozsa, A. Pere, W.K. Wootters, Teleporting an unknown quantum state via dual classical and Einstein–Podolsky–Rosen channels. *Phys. Rev. Lett.* **70**, 1895–1899 (1993)
9. A.K. Pati, Minimum classical bit for remote preparation and measurement of a qubit. *Phys. Rev. A* **63**, 014302 (2000)
10. C.H. Bennett, D.P. DiVincenzo, P.W. Shor et al., Remote state preparation. *Phys. Rev. Lett.* **87**, 077902 (2001)
11. D.W. Berry, B.C. Sanders, Optimal remote state preparation. *Phys. Rev. Lett.* **90**, 057901 (2003)
12. I. Devetak, T. Berger, Low-entanglement remote state preparation. *Phys. Rev. Lett.* **87**, 197901 (2001)
13. A. Hayashi, T. Hashimoto, M. Horibe, Remote state preparation without oblivious conditions. *Phys. Rev. A* **67**, 052302 (2003)
14. D.W. Leung, P.W. Shor, Oblivious remote state preparation. *Phys. Rev. Lett.* **90**, 127905 (2003)
15. J.Y. Peng, Remote preparation of general one-, two- and three-qubit states via χ -type entangled states. *Int. J. Theor. Phys.* **59**, 3789–3803 (2020)
16. P.E. Tressoldi, A. Khrennikov, Remote state preparation of mental information: a theoretical model and a summary of experimental evidence. *Soc. Sci. Electron. Publ.* **10**(3), 54–60 (2012)
17. X.H. Peng, X.W. Zhu, X.M. Fang et al., Experimental implementation of remote state preparation by nuclear magnetic resonance. *Phys. Lett. A* **306**(5–6), 271–276 (2003)
18. M.X. Luo, X.B. Chen, Y.X. Yang et al., Experimental architecture of JRSP. *Quantum Inf. Process.* **11**(3), 751–767 (2012)
19. B.A. Nguyen, J. Kim, JRSP. *J. Phys. B At. Mol. Opt. Phys.* **41**, 095501 (2008)
20. J.Y. Peng, M.X. Luo, Z.W. Mo, Flexible deterministic JRSP of some states. *Int. J. Quantum Inf.* **11**, 1350044 (2013)
21. B.A. Nguyen, T.B. Cao, V.D. Nung, Deterministic JRSP. *Phys. Lett. A* **375**, 3570–3573 (2011)
22. Q.Q. Chen, Y. Xia, J. Song, Deterministic joint remote preparation of an arbitrary three-qubit state via EPR pairs. *J. Phys. A Math. Theor.* **45**, 055303 (2012)
23. M.X. Luo, X.B. Chen, S.Y. Ma et al., Joint remote preparation of an arbitrary three-qubit state. *Opt. Commun.* **283**, 4796–4801 (2010)
24. J.Y. Peng, M.X. Luo, Z.W. Mo, Joint remote state preparation of arbitrary two-particle states via GHZ-type states. *Quantum Inf. Process.* **12**, 2325–2342 (2013)
25. B.A. Nguyen, JRSP via W and W-type states. *Opt. Commun.* **383**, 4113–4117 (2010)
26. M.M. Wang, X.B. Chen, Y.X. Yang, Deterministic joint remote preparation of an arbitrary two-qubit state using the cluster state. *Commun. Theor. Phys.* **59**, 568–572 (2013)
27. X.Q. Xiao, J.M. Liu, G.H. Zeng, JRSP of arbitrary two- and three-qubit states. *J. Phys. B At. Mol. Opt. Phys.* **44**, 075501 (2011)
28. Q. Chen, Y. Xia, Joint remote preparation of arbitrary two-qubit state via a generalized seven-qubit Brown state. *Laser Phys.* **26**, 015203 (2016)
29. J.Y. Peng, M.Q. Bai, Z.W. Mo, JRSP of a four-dimensional quantum state. *Chin. Phys. Lett.* **31**, 010301 (2014)
30. M.X. Ding, M. Jiang, Deterministic joint remote preparation of an arbitrary seven-qubit cluster-type state. *Int. J. Theor. Phys.* **56**, 1875–1882 (2017)
31. W.Q. Li, H.W. Chen, Z.H. Liu, Deterministic joint remote preparation of arbitrary four-qubit cluster-type state using EPR pairs. *Int. J. Theor. Phys.* **56**, 351–361 (2017)
32. C. Hao, B. Gui et al., Efficient schemes for deterministic joint remote preparation of an arbitrary four-qubit W-type entangled state. *Pramana J. Phys.* **88**, 82 (2017)
33. Z.H. Wei, X.W. Zha, Y. Yu, Efficient schemes of remote state preparation for two-qubit equatorial states. *Int. J. Theor. Phys.* **55**, 5046–5054 (2016)
34. T. Cai, M. Jiang, Optimal JRSP of arbitrary equatorial multi-qubit states. *Int. J. Theor. Phys.* **56**, 781–781 (2017)
35. B.A. Nguyen, J. Kim, Nonstandard protocols for joint remote preparation of a general quantum state hybrid entanglement of any dimension. *Phys. Rev. A* **98**, 042329 (2018)

36. R.F. Yu, Y.J. Liu, P. Zhou, Joint remote preparation of arbitrary two- and three-photon state with linear-optical elements. *Quantum Inf. Process.* **15**, 4785–47803 (2016)
37. C.H. Bennet, P.W. Shor, Quantum information theory. *IEEE Trans. Inf. Theory* **44**, 2724–2742 (2002)
38. Z.F. Chen, J.M. Liu, L. Ma et al., Deterministic joint remote preparation of an arbitrary two-qubit state in the presence of noise. *Chin. Phys. B* **23**, 020312 (2014)
39. M.M. Wang, Z.G. Qu, W. Wang, J.G. Chen, Effect of noise on deterministic joint remote preparation of an arbitrary two-qubit state. *Quantum Inf. Process.* **16**, 140 (2017)
40. X.W. Guan, X.B. Chen, L.C. Wang et al., Joint remote preparation of an arbitrary two-qubit state in noisy environments. *Int. J. Theor. Phys.* **53**, 2236–2245 (2014)
41. H.Q. Liang, J.M. Liu, S.S. Feng et al., Effect of noises on JRSP via a GHZ-class channel. *Quantum Inf. Process.* **14**(10), 3857–3877 (2015)
42. M.M. Wang, Z.G. Qu, Effect of noise on deterministic JRSP of a qubit state via a GHZ channel. *Quantum Inf. Process.* **15**, 4805–4818 (2016)
43. B.J. Falaye, G.H. Sun, JRSP of three-particle state via three tripartite GHZ class in quantum noisy channels. *Int. J. Quantum Inf.* **14**, 1650034 (2016)
44. A.G. Adepou, B.J. Falaye, G.H. Sun et al., JRSP (JRSP) of two-qubit equatorial state in quantum noisy channels. *Phys. Lett. A* **381**, 581–587 (2017)
45. H.X. Zhao, L. Huang, Effect of noise on JRSP of an arbitrary equatorial two-qubit state. *Int. J. Theor. Phys.* **56**, 720–728 (2017)
46. S. Chitra, T. Kishore, P. Anirban, Hierarchical JRSP in noisy environment. *Quantum Inf. Process.* **16**, 205 (2017)
47. C. Macchiavello, G.M. Palma, Entanglement-enhanced information transmission over a quantum channel with correlated noise. *Phys. Rev. A* **65**, 050301 (2002)
48. M.B. Plenio, S. Virmani, Spin chains and channels with memory. *Phys. Rev. Lett.* **99**, 120504 (2007)
49. A. D'Arrigo, G. Benenti, G. Falci, C. Macchiavello, Classical and quantum capacities of a fully correlated AD channel. *Phys. Rev. A* **88**, 042337 (2013)
50. F. Caruso, V. Giovannetti, C. Lupo, S. Mancini, Quantum channels and memory effect. *Rev. Mod. Phys.* **86**, 1203 (2014)
51. X. Xiao, Y. Yao, Y.L. Li, Y.M. Xie, X.H. Wang, Protecting entanglement from correlated AD channel using weak measurement and quantum measurement reversal. *Quantum Inf. Process.* **15**, 3881–3891 (2016)
52. J. Du, R. Xing, Z. Nan et al., Preserving electron spin coherence in solids by optimal dynamical decoupling. *Nature* **461**(7268), 1265–1268 (2009)
53. C.C. Luo, L. Zhou, W. Zhong et al., Multipartite entanglement purification using time-bin entanglement. *Laser Phys. Lett.* **18**(6), 065205 (2021)
54. A. Chiesa, F. Petiziol, M. Chizzini et al., Theoretical design of optimal molecular qudits for quantum error correction. *J. Phys. Chem. Lett.* **28**, 13 (2022)
55. A.P. Liu, L.Y. Cheng, L. Chen et al., Quantum information processing in decoherence-free subspace with nitrogen-vacancy centers coupled to a whispering-gallery mode microresonator. *Opt. Commun.* **313**, 180–185 (2014)
56. Y.L. Li, X. Xiao, Recovering quantum correlations from AD decoherence by weak measurement reversal. *Quantum Inf. Process.* **12**, 3067–3077 (2013)
57. J.Y. Peng, Y. Xiang, Bidirectional remote state preparation in noisy environment assisted by weak measurement. *Opt. Commun.* **499**, 127285 (2021)
58. S. Ashhab, F. Nori, Control-free control: manipulating a quantum system using only a limited set of measurements. *Phys. Rev. A* **82**, 062103 (2010)
59. J.Y. Peng, L. Tang, Z. Yang et al., Cyclic teleportation in noisy channel with nondemolition parity analysis and weak measurement. *Quantum Inf. Process.* **21**, 114 (2022)
60. L. LiY, Y. Yao, X. Xiao, Robust quantum state transfer between two superconducting qubits via partial measurement. *Laser Phys. Lett.* **13**, 125202 (2016)
61. Y.S. Kim, J.C. Lee, Protecting entanglement from decoherence using weak measurement and quantum measurement reversal. *Nat. Phys.* **8**, 117–120 (2012)
62. W. Li, H. Zhi, Q. Wang, Protecting distribution entanglement for two-qubit state using weak measurement and reversal. *Int. J. Theor. Phys.* **56**(9), 1–12 (2017)
63. M.J. Wang, Y.J. Xia, Y. Yang et al., Protecting the entanglement of two-qubit over quantum channels with memory via weak measurement and quantum measurement reversal. *Chin. Phys. B* **29**(11), 110307 (2020)
64. Y. Yeo, A. Skeen, Time-correlated quantum amplitude-damping channel. *Phys. Rev. A* **67**, 064301 (2003)
65. A.N. Korotkov, A.N. Jordan, Undoing a weak quantum measurement of a solid-state qubit. *Phys. Rev. Lett.* **97**, 166805 (2006)
66. N. Katz, M. Neeley, M. Ansmann, R.C. Bialczak et al., Reversal of the weak measurement of a quantum state in a superconducting phase qubit. *Phys. Rev. Lett.* **101**, 200401 (2008)
67. Y.S. Kim, Y.W. Cho, Y.S. Ra et al., Reversing the weak quantum measurement for a photonic qubit. *Opt. Express* **17**(14), 1197811985 (2009)
68. Y.S. Kim, J.C. Lee, O. Kwon, Y.H. Kim, Protecting entanglement from decoherence using weak measurement and quantum measurement reversal. *Nat. Phys.* **8**(2), 11712 (2012)
69. J.C. Lee, Y.C. Jeong, Y.S. Kim, Y.H. Kim, Experimental demonstration of decoherence suppression via quantum measurement reversal. *Opt. Express* **19**(17), 1630916316 (2011)

Springer Nature or its licensor (e.g. a society or other partner) holds exclusive rights to this article under a publishing agreement with the author(s) or other rightsholder(s); author self-archiving of the accepted manuscript version of this article is solely governed by the terms of such publishing agreement and applicable law.